UNSTEADY SEPARATION EXPERIMENTS ON 2-D AIRFOILS, 3-D WINGS, AND MODEL HELICOPTER ROTORS

Peter F. Lorber and Franklin O. Carta
United Technologies Research Center
East Hartford, CT 06108

ABSTRACT FOR NASA/AFOSR/ARO WORKSHOP ON
PHYSICS OF FORCED UNSTEADY SEPARATION
APRIL 17-19, 1990

Information on unsteady separation and dynamic stall is being obtained from two experimental programs that have been underway at United Technologies Research Center since 1984. The first program is designed to obtain detailed surface pressure and boundary layer condition information during high amplitude pitching oscillations of a large (17.3 in chord) model wing in a wind tunnel. The second program involves the construction and testing of a pressure-instrumented model helicopter rotor. This presentation describes some of the results of these experiments, and in particular compares the detailed dynamic stall inception information obtained from the oscillating wing with the unsteady separation and reverse flow results measured on the retreating blade side of the model rotor during wind tunnel testing.

An inital, two-dimensional oscillating wing experiment was performed in 1986 under AFOSR sponsorship, and has been documented in Refs. 1 and 2. Surface pressure and hot film data were acquired for constant pitch rate ramps and sinusoidal oscillations in the range of α = 0 to 30 deg, for M = 0.2, 0.3, and 0.4, and Re = 2,000,000 to 4,000,000. Figure 1 shows typical results for an M = 0.2, A = $\dot{\alpha}c/2U_\infty$ = 0.01 ramp. This figure is similar to those in Refs. 1 and 2, and shows time histories of the ensemble-averaged pressures at each of the 18 transducers on the airfoil surface. A negative pressure spike (caused by the dynaic stall vortex) forms near τ = 0.47, and moves back along the airfoil. Figure 2 (not previously published) shows chordwise pressure distributions at several values of τ during this process. The passage of the vortex is shown by the pressure bulge on the upper surface. The references discuss the effects of pitch rate, pitching waveform, and Mach number on the stall process. Compressibility effects were very significant, as a small supersonic bubble forms near the leading edge at M = 0.4, and the peak suction pressures and the unsteady increments to the airlods are much weaker. Reference 3 describes a Navier-Stokes simulation of the 2-D experiments. Good agreement was obtained up through the formation of the dynamic stall vortex, while many of the quantitative aspects of the periodic vortex shedding after stall were missed.

This study is now being extended under ARO and AFOSR sponsorship to include three-dimensional measurements on a finite tip model. In addition to obtaining information on how the presence of the wing tip affects the dynamic stall process, this experiment is intended to study sweep and compressibility effects. The model, shown in Fig. 3, consists of a square wing with the same (17.3 in) chord and airfoil section (SSC-A09) as the 2-D wing. The instrumentation consists of chordwise arrays of pressure transducers at 5 spanwise stations (112

transducers) and arrays of surface hot film gages at 3 spanwise stations (16 total gages) to determine transistion and separation information. The model will be tested at 3 sweep angles: Λ = 0, 15, and 30 deg, and at Mach numbers between 0.2 and (structural loads permitting) 0.6. The experiment is scheduled to be completed in 1990.

In addition to large amplitude ramps and sinusoids, information will be obtained on small amplitude ($\pm$0.5 to 2 deg) oscillations near the static stall angle. This program will be sponsored by NASA Lewis and ARO, and is designed to study the incipient stages of stall flutter, with particular application to aircraft propellors. Results of an earlier, smaller scale experiment were reported in Ref. 4. The aerodynamic damping was found to be substantially more negative for very small amplitude oscillations, allowing a rapid growth to a limit cycle motion.

The helicopter rotor program involves the construction and testing of a heavily instrumented, 9.5 ft diameter scale model of a current-technology main rotor (Fig. 4). The model contains 176 miniature pressure transducers, as well as strain gages, temperature sensors, and surface hot film gages. Hover testing was described in Ref. 5, and aerodynamic results from a 1989 wind tunnel test are given in Ref. 6. A great deal of information has been obtained using this model rotor. Of current interest is the behavior of the inboard portion of the retreating blade at moderately high advance ratios ($\mu = U_\infty/\Omega R \sim 0.28$-$0.36$). This region is subject to rapid increases in angle of attack and rapid reductions in relative velocity. Figure 5 shows chordwise pressure distributions for r/R = 0.4 at four azimuths on the retreating side. The flow appears highly loaded but attached at ψ = 190, shows leading edge separation at at ψ = 220, has a very large aft loading at ψ = 270, and is beginning to reattach at ψ = 320. Time histories of the ensemble averaged pressures at r/R = 0.225 and 0.4 are shown in Fig. 6. Sharp negative pressure spikes are present (on the upper surface only) near ψ = 175 at r/R = 0.225 and near ψ = 210 at r/R = 0.4. The flow appears to separate after the spikes have passed, as shown by flat ensemble averaged pressures between ψ = 180 and 315. This phenomenon is similar to the shedding of the dynamic stall vortex on the oscillating 2-D airfoil (Fig. 1). The non-dimensional convection speed of the spike (0.25 times the local relative velocity) is also similar.

The rotor flow field has many complexities not present with the 2-D airfoil. The sequence observed on the retreating blade side at a particular radial station may include: forming and shedding a leading edge vortex, entering the region of reverse relative velocity, shifting from positive to negative lift, shedding a vortex from the trailing edge that moves towards the leading edge, resuming positive relative velocity and lift, and interacting with the wake of the rotor hub. Additional complications include radial velocity and twist gradients and aeroelastic deflections. With all of these factors present, it is encouraging to see some similarities to the simpler, oscillating 2-D results, but one must not forget how complex the rotor flow field actually is. This observation is lent particular weight by the many references to the helicopter stall problem in the introductory sections of oscillating airfoil papers.

References

1. Lorber, P.F., and Carta, F.O., "Airfoil Dynamic Stall at Constant pitch Rate and High reynolds Number," AIAA J. Aircraft, Vol 25, pp. 548-556, June 1988.

2. Lorber, P.F., and Carta, F.O., "Unsteady Stall Penetration Experiments at High Reynolds Number," AFOSR TR-87-1202, April 1987.

3. Patterson, M.T., and Lorber, P.F., "Computational and Experimental Studies of Compressible Dynamic Stall," 4th Symposium on Numerical and Physical Aspects of Aerodynamic Flows, Long Beach, CA, Jan 1989 (accepted for publication in the J. Fluids & Structures, 1990).

4. Carta, F.O., and Lorber, P.F., "Experimental Study of the Aerodynamics of Incipient Torsional Stall Flutter," AIAA J. Propulsion and Power, Vol. 3, pp.164-170, March-April, 1987.

5. Lorber, P.F., Stauter, R.C., and Landgrebe, A.J., "A Comprehensive Hover Test of the Airloads and Airflow of an Extensively Instrumented Model Helicopter Rotor," 45th Annual Forum of the American Helicopter Society, Boston, MA, May 1989.

6. Lorber, P.F., "Aerodynamic Results of a Pressure-Instrumented Model Rotor Test at the DNW," to be presented at the 46th Annual Forum of the American Helicopter Society, Washington, DC, May 1990.

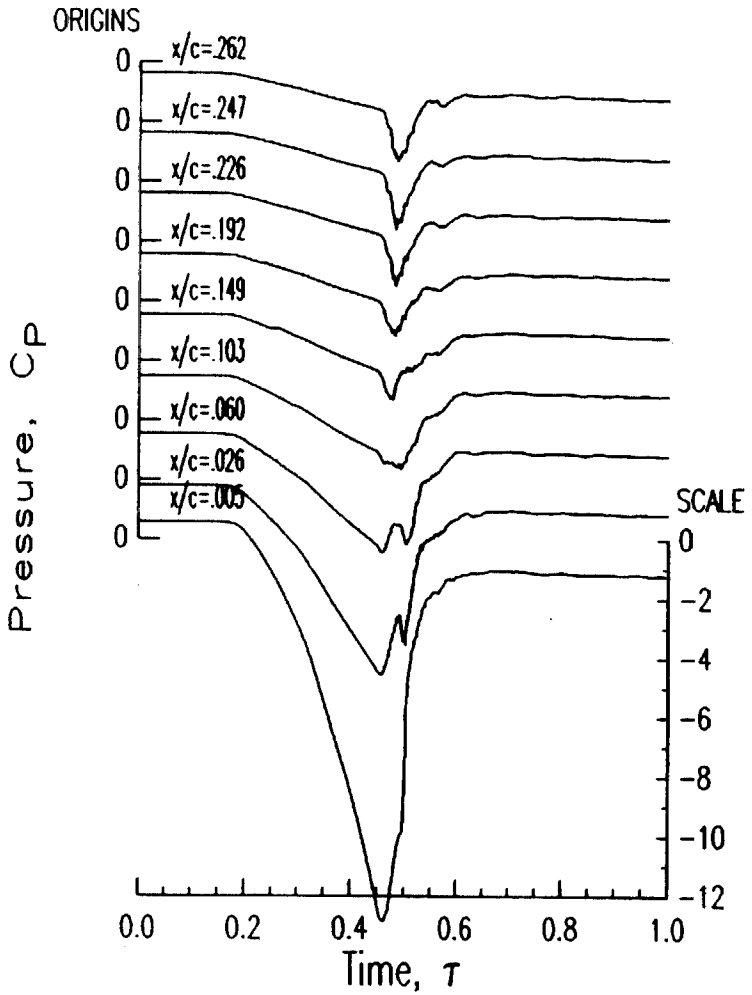

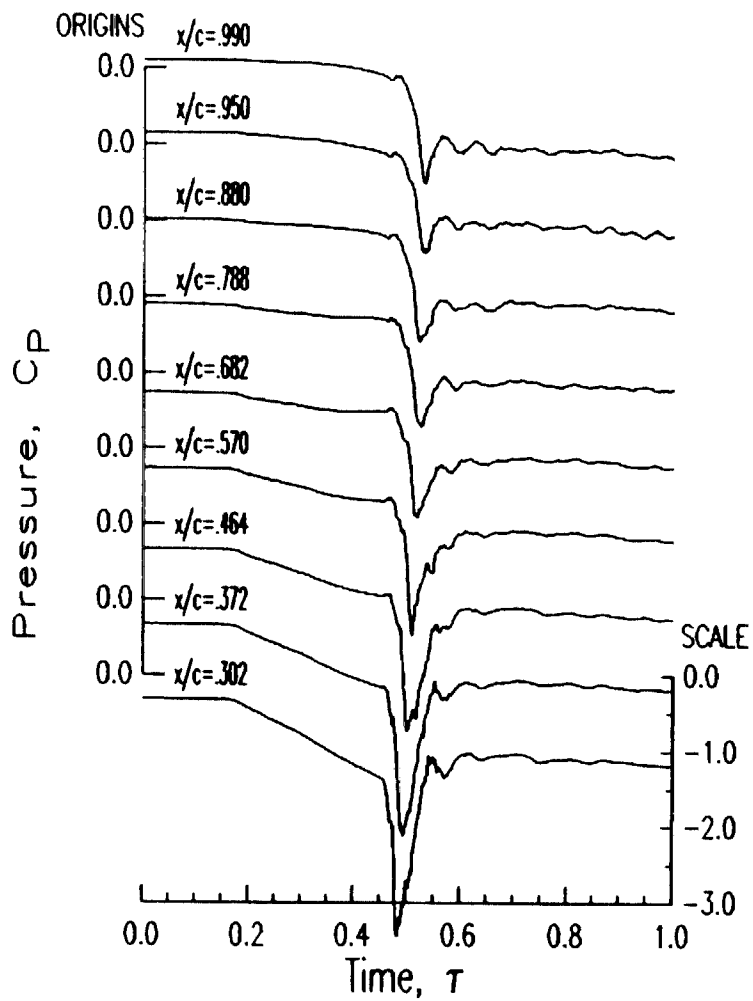

Figure 1. Pressure time histories showing dynamic stall on the 2-D oscillating wing.

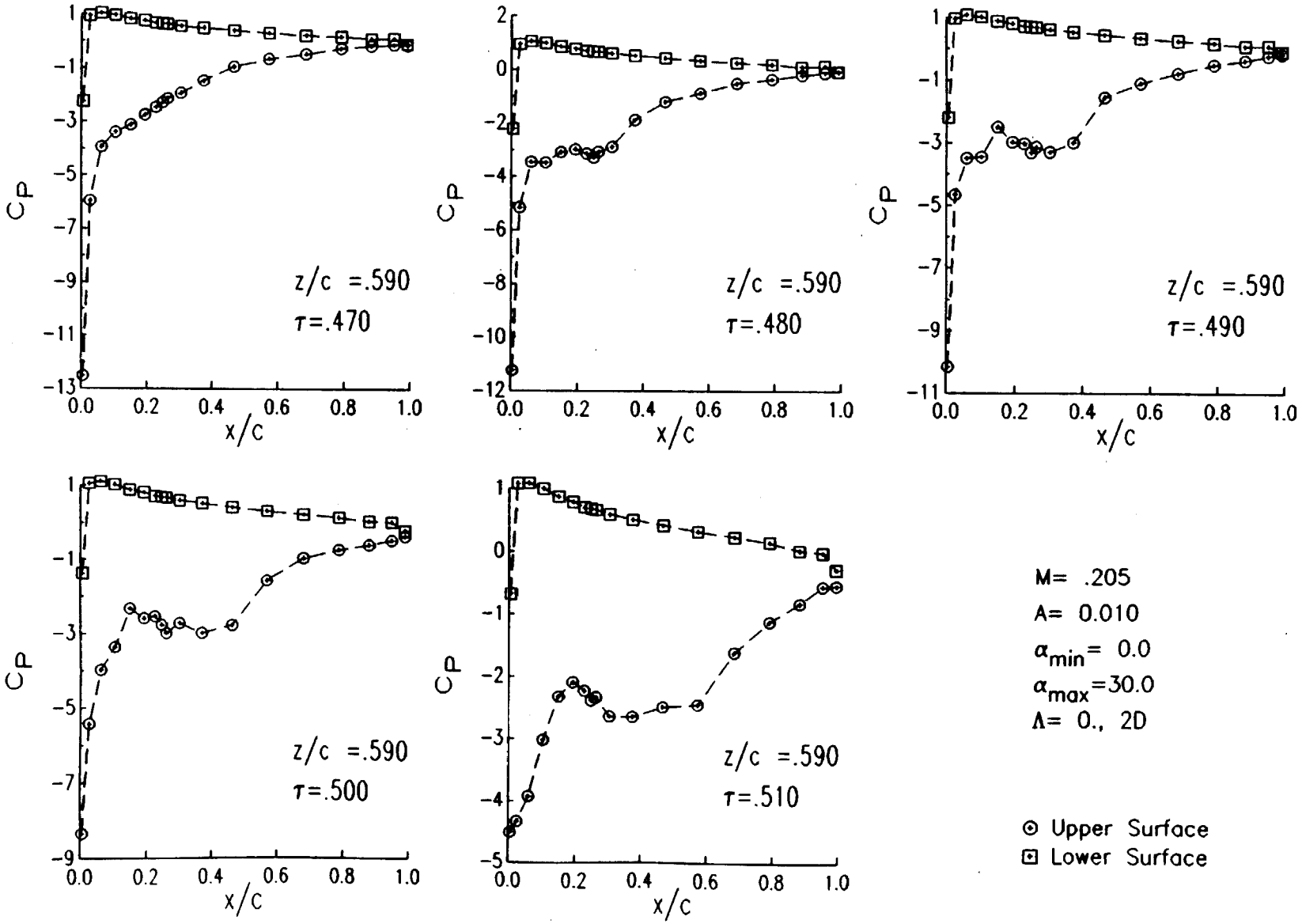

Figure 2. Chordwise pressure distributions showing propagation of the dynamic stall vortex on the 2-D oscillating wing.

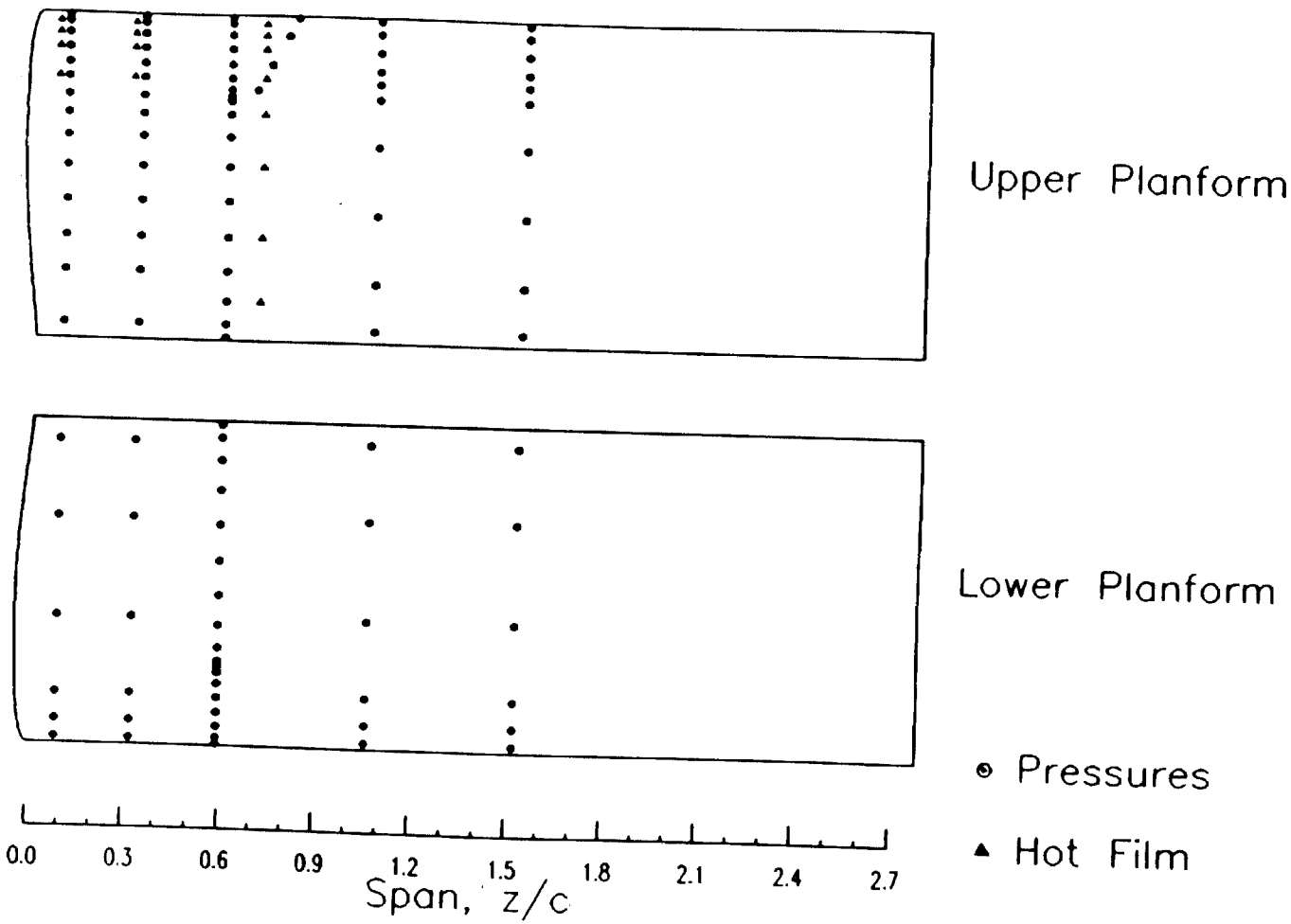

Figure 3. 3-D oscillating wing planform and instrumentation layout.

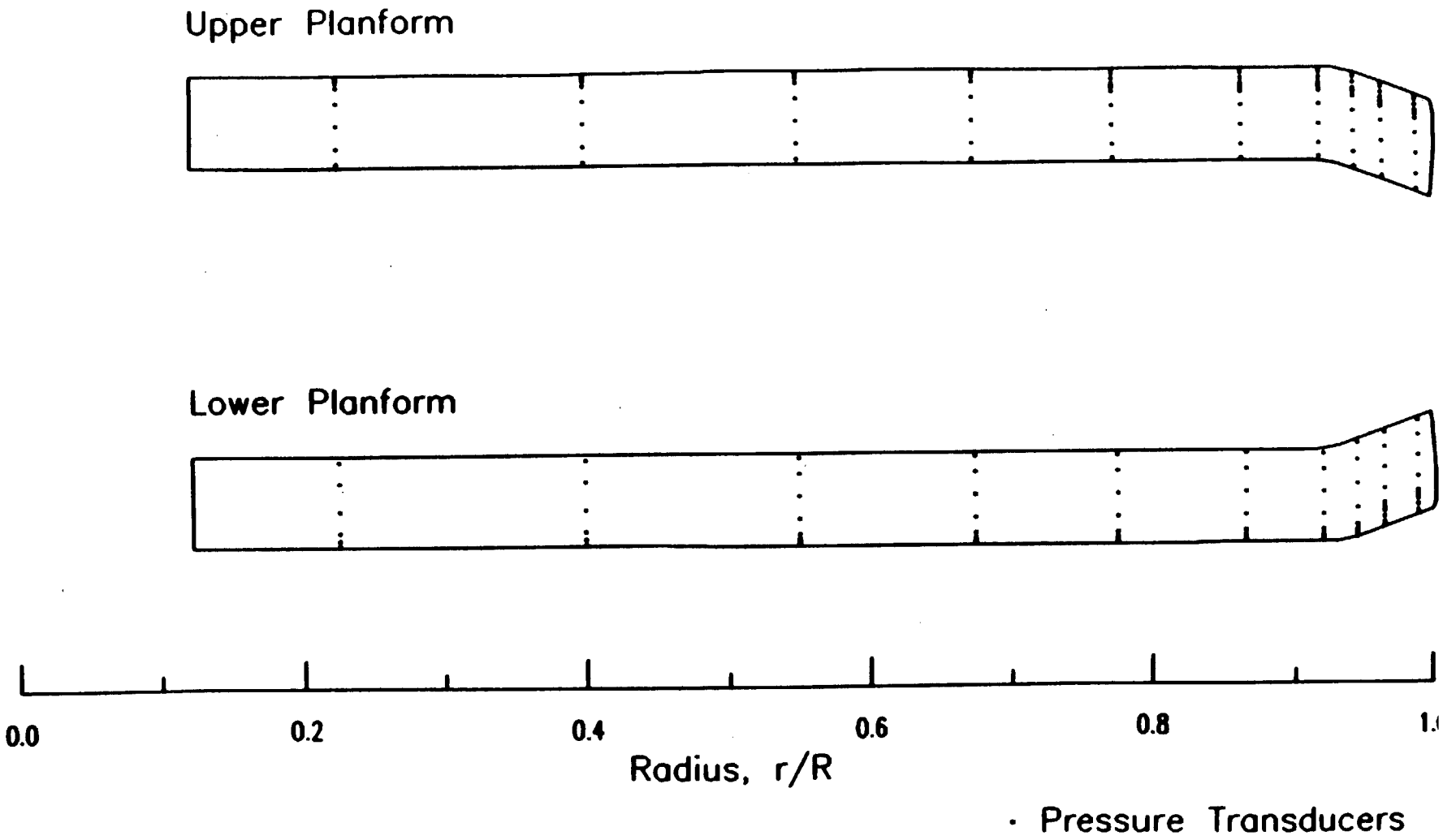

Figure 4. Model helicopter rotor planform and instrumentation layout.

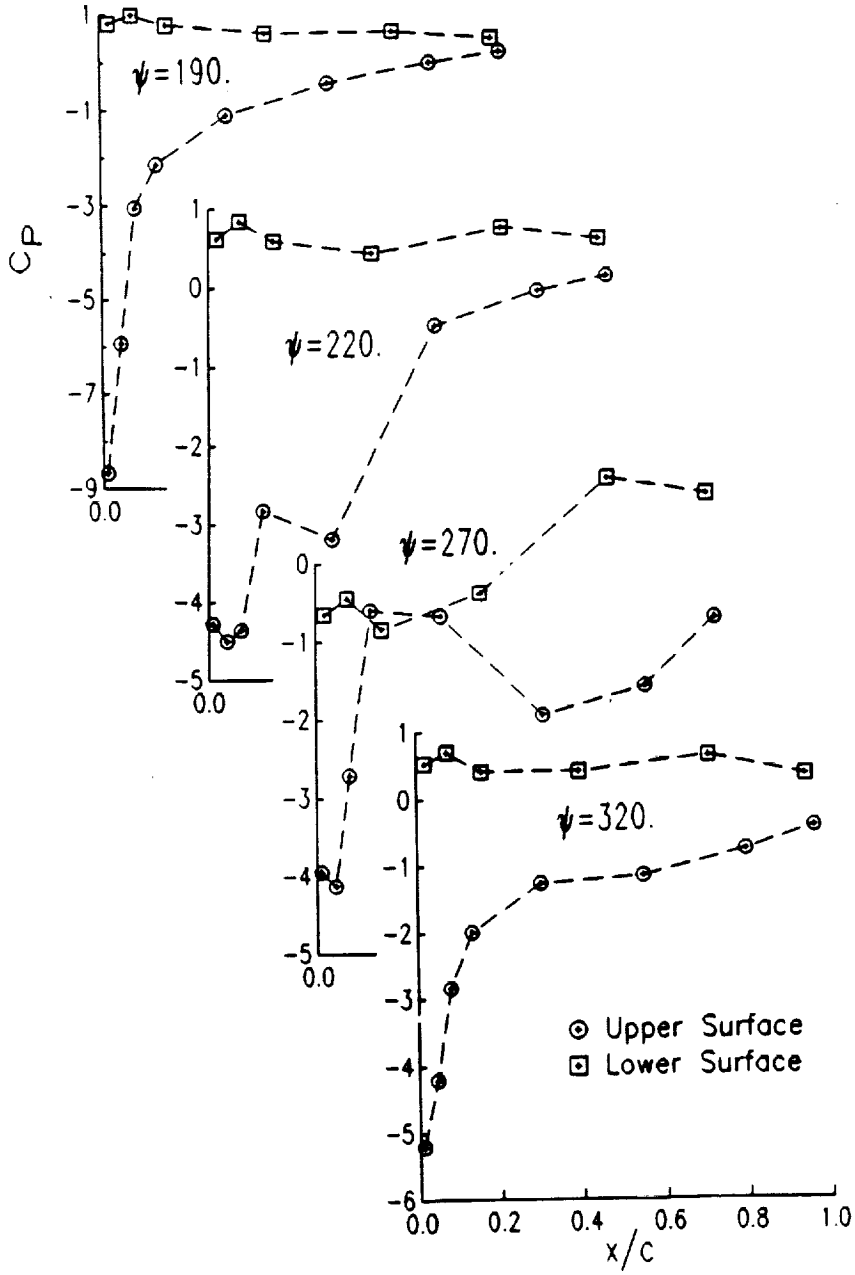

Figure 5. Chordwise pressure distributions on the model helicopter rotor, showing the separation process at r/R = 0.4.

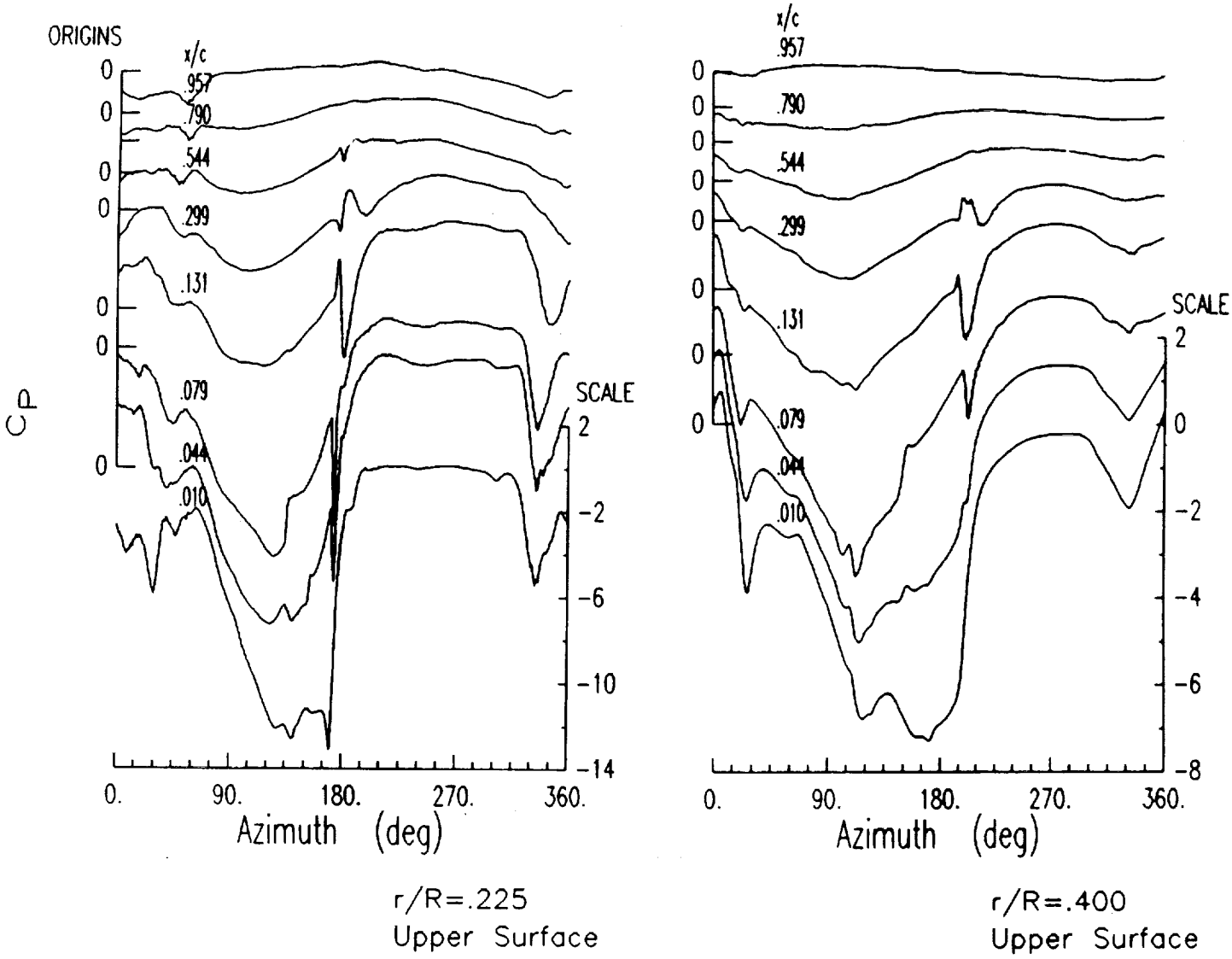

Figure 6. Pressure time histories on the model helicopter rotor, showing vortex formation and flow separation.

2-D AIRFOIL EXPERIMENT

- Pressure and Hot Film Instrumented 8 ft Span Wing
- Sikorsky SSC-A09 9% thick airfoil
- M = 0.2, 0.3, 0.4
- Re = 2 to 4 million (c = 17.3 in)
- $\alpha = 0.0 \Rightarrow 30.0$ deg Ramps and Sinusoids
- $A = \frac{\dot{\alpha} c}{2U} = 0.001$ to 0.02
- 1986 Test under AFOSR Sponsorship

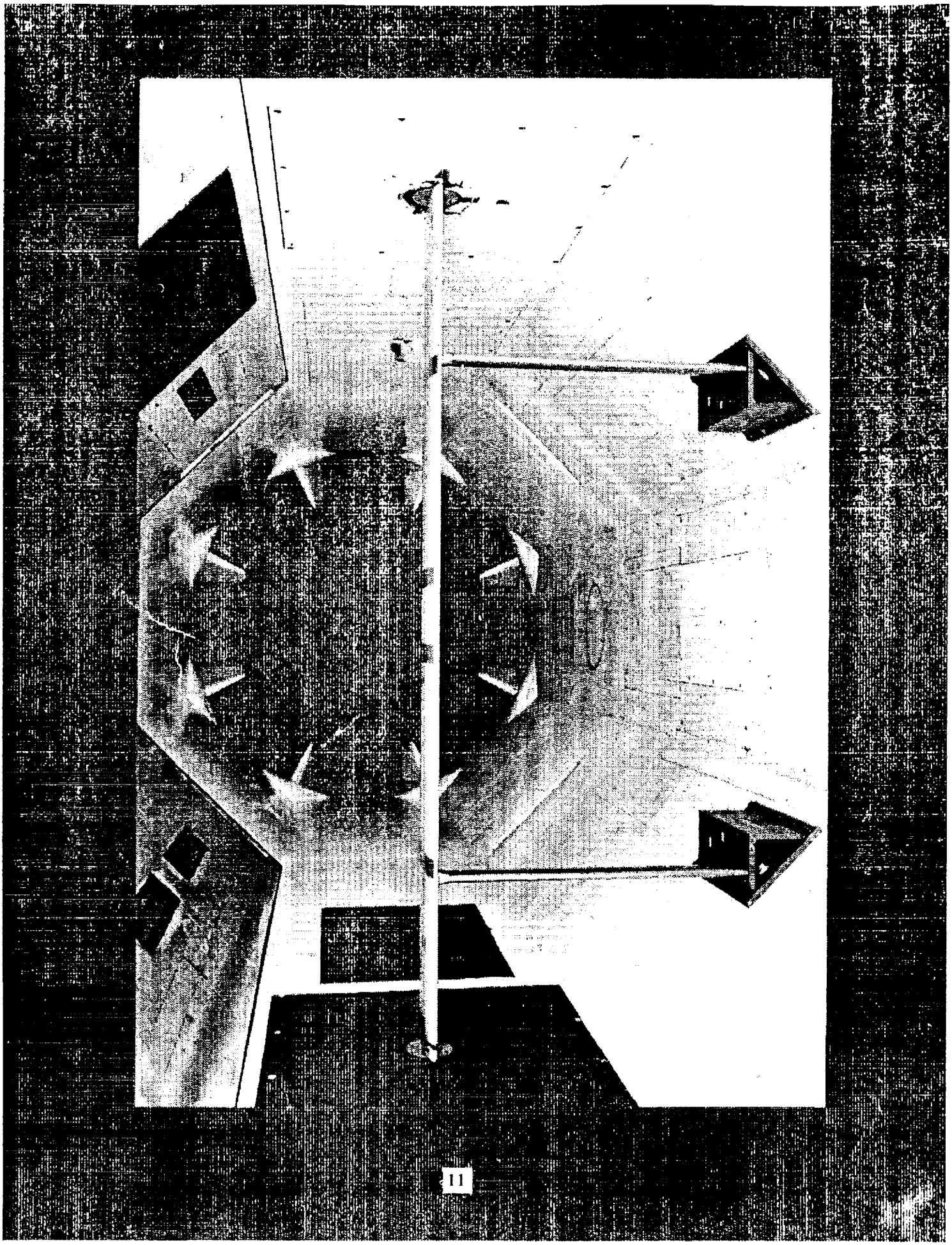

AIRFOIL CONSTANT-PITCH-RATE MOTION

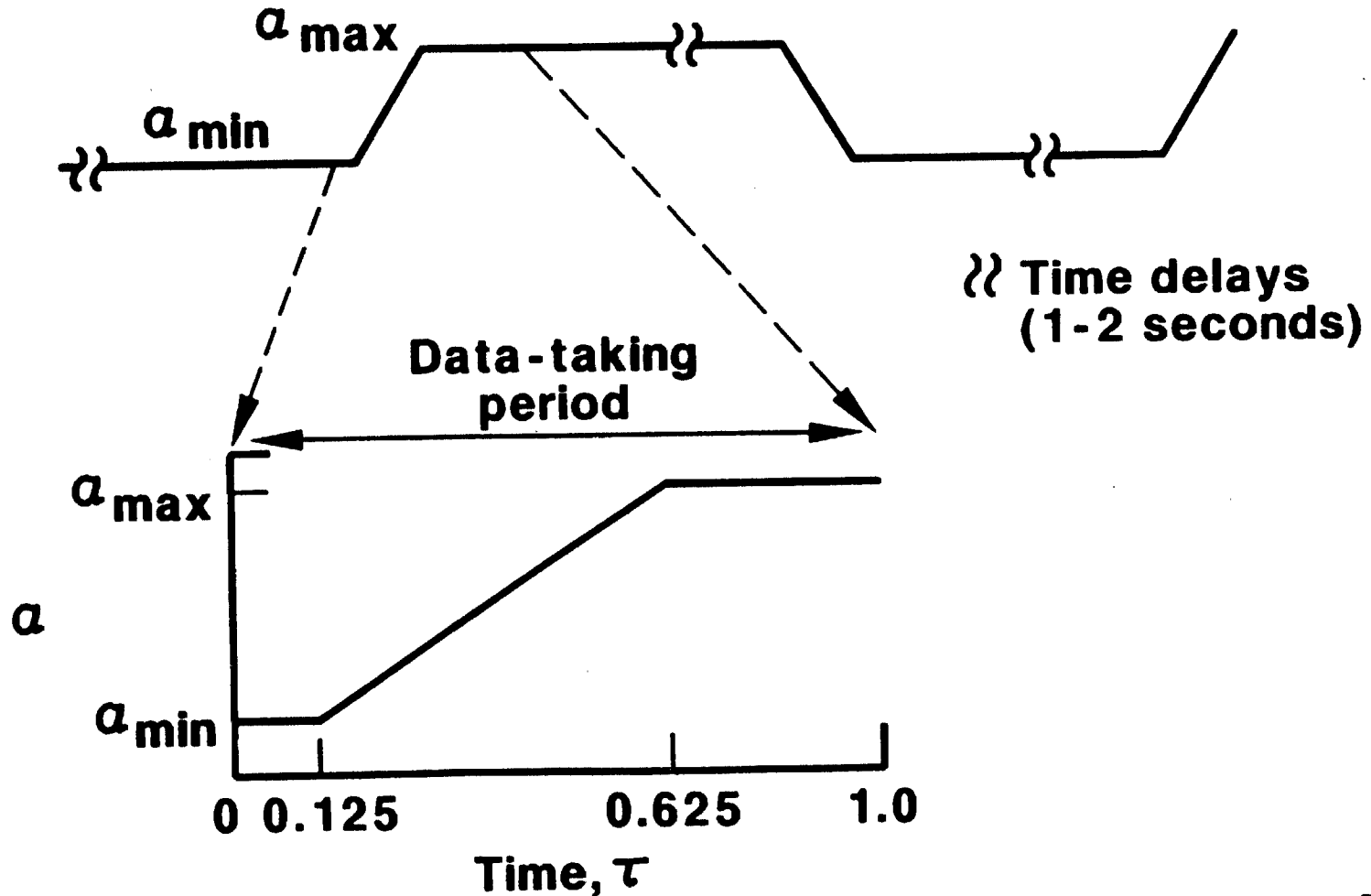

RD1199ETX.001

2-D AIRFOIL COMPUTATIONS

- Compressible Navier-Stokes Method (NS2D by Sankar, et. al)
- Computations Made by Patterson (1988) at M=0.2 and 0.4
- Correctly Predicts Lift Slope, Peak Lift, and Stall Angle
- Correctly Predicts Reduced Lift and Earlier Stall at M=0.2
- Overpredicts Post-stall Vortex Shedding
- Smears Shock near Leading Edge

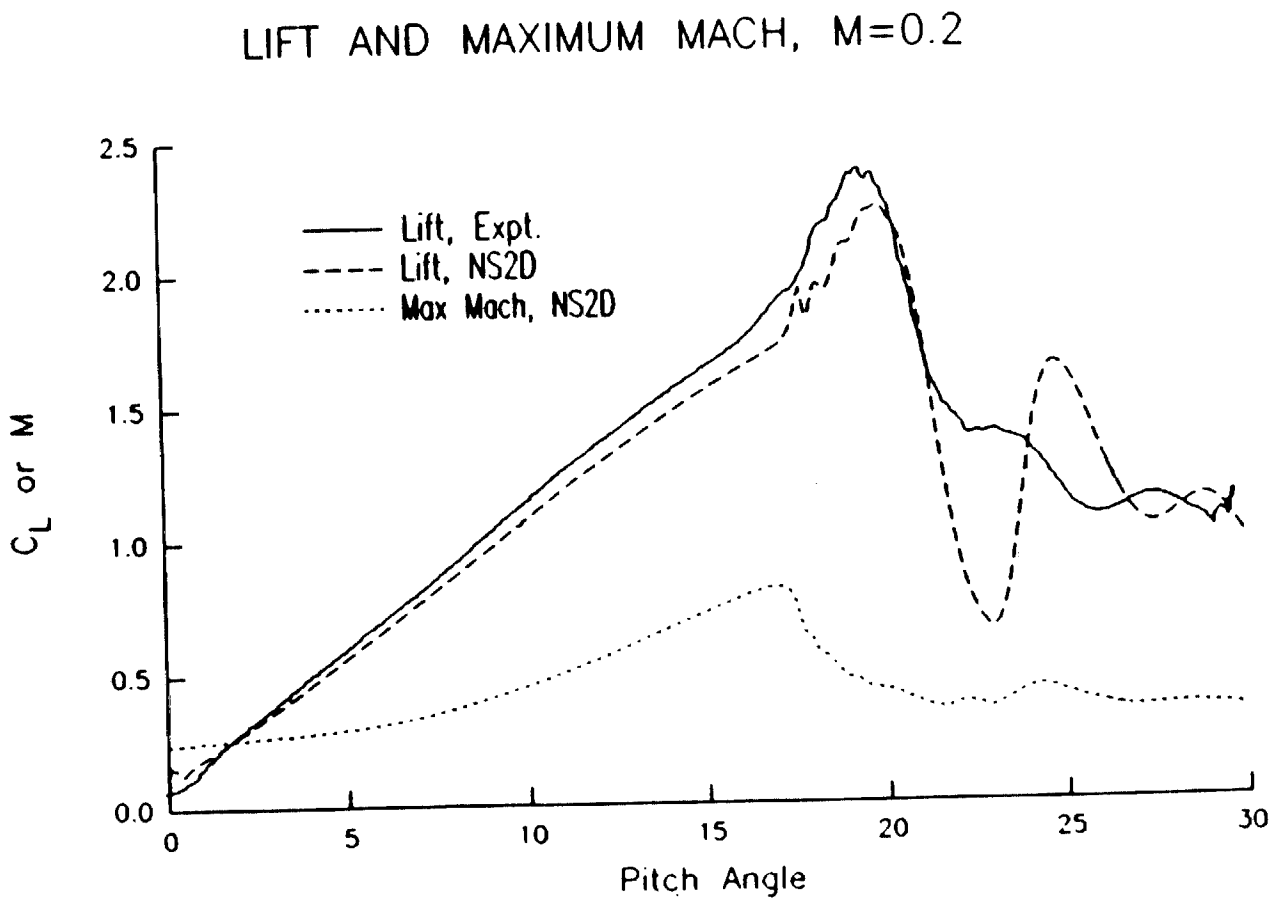
LIFT AND MAXIMUM MACH, M=0.2
Lift, Expt.
Lift, NS2D
Max Mach, NS2D
C_L or M
2.5
2.0
1.5
1.0
0.5
0.0
0
5
10
15
20
25
30
Pitch Angle

3-D OSCILLATING WING EXPERIMENT

- Pressure and Hot Film Instrumented 4 ft Span Wing
- Sikorsky SSC-A09 9% thick airfoil
- M = 0.2, 0.3, 0.4, 0.5, 0.6
- $\Lambda = 0, 15, 30$ deg
- Re = 2 to 6 million (c = 17.3 in)
- $\alpha = 0.0 \Rightarrow 30.0$ deg Ramps and Sinusoids
- $A = \frac{\dot{\alpha} c}{2U} = 0.001$ to 0.02 or 0.04
- 1990 Test under ARO/AFOSR Sponsorship

INCIPIENT STALL EXPERIMENT

- Application to Stall Flutter of Propellers
- Small Amplitude Oscillations near Static Stall
- Preliminary Experiment in Small Wind Tunnel in 1984
- Amplitudes of 0.5, 2.0 and 4.0 deg at M=0.18
- Saw Increased Negative Pitch Damping at Small Amplitude

INCIPIENT STALL EXPERIMENT - FUTURE

- NASA Lewis Sponsored Addition to 3-D Oscillating Wing Test
- Improved Resolution of Pressures
- Improved Flow Quality
- Higher Mach Numbers and Frequencies
- Addition of 3-D Tip and Sweep Effects

MODEL HELICOPTER ROTOR EXPERIMENT

- 1989 Joint UTRC/Army/NASA/Sikorsky Test at DNW, Holland
- Measured Aerodynamics, Acoustics, Performance, & Dynamics
- Pressure-Instrumented 9.4ft Dia. Model of Sikorsky Main Rotor
- Mach and Aeroelastically Scaled
- Data from 109 Level Flight, Descent, and Hover Conditions

ROTOR TEST INSTRUMENTATION

- 176 Blade Pressure Transducers
- 19 In-Flow and Out-of-Flow Microphones
- 16 Blade Bending and Torsion Strain Gages
- 3 Blade Control Angles and 4 Control Loads
- 7 Rotor Balance and Torque Loads
- Shaft Angle, RPM, and Wind Tunnel Conditions

AERODYNAMIC COEFFICIENT DEFINITIONS

- Surface Pressure Coefficient

$$C'_P(x,r,\psi) = \frac{P(x,r,\psi)-P_\infty}{0.5\rho_\infty(\Omega r)^2}$$

$$C_P(x,r,\psi) = \frac{P(x,r,\psi)-P_\infty}{0.5\rho_\infty(\Omega r(1+\frac{\mu R}{r}sin(\psi-\lambda)))^2}$$

- Normal Force Coefficient (Blade Section Axes)

$$C_N(r,\psi) = \frac{\partial N/\partial r}{0.5\rho_\infty(\Omega r(1+\frac{\mu R}{r}sin(\psi-\lambda)))^2 c(r)}$$

- Section Thrust Coefficient (Shaft Axes)

$$C_t(r,\psi) = \frac{\partial t/\partial r}{0.5\rho_\infty(\Omega R)^2 c}$$

MODEL HELICOPTER ROTOR RETREATING SIDE EVENTS

- Inboard Leading Edge Vortex Shedding Similar to 2-D Airfoil
- Aerodynamics Complicated by:
  1. Reverse Flow
  2. Radial Gradients in Velocity and Twist
  3. Streamwise Velocity and Flapping Oscillations
  4. Wake Interactions

RETREATING SIDE EVENTS - $\mu = 0.30$